First-Principles Calculation on Geometric, Electronic and Optical Properties of Fully Fluorinated Stanene: a Large-Gap Quantum Spin Hall Insulator *

Hong Wu(武红)[1], Feng Li(李峰)[2]**

[1]*Department of Physics, Nanjing University of Posts and Telecommunications, Nanjing 210023*
[2]*College of Chemistry and Materials Science, Jiangsu Key Laboratory of Biofunctional Materials, Nanjing Normal University, Nanjing 210023*

(Received 13 January 2016)

The searches for large-gap quantum spin Hall insulators are important for both practical and fundamental interests. In this work, we present a theoretical observation of the two-dimensional fully fluorinated stanene (SnF) by means of density functional theory. Remarkably, a significant spin-orbit coupling is observed for the SnF monolayer in the valence band at the Γ point, with a considerable indirect band gap of 278 meV. The direct gap of the SnF monolayer is at the Γ point, which is slightly larger by as much as 381 meV. In addition, the elastic modulus of the SnF monolayer is about 20 J/m^2, which is comparable with the in-plane stiffness of black phosphorus monolayer along the x-direction ($\sim$28.94 J/m^2). Finally, the optical properties of stanene, SnF monolayer and stanene/SnF bilayer are calculated, in which the stanene/SnF bilayer is supposed to be an attractive sunlight absorber.

PACS: 71.20.Gj, 73.61.−r, 78.20.−e DOI: 10.1088/0256-307X/33/6/067101

Following the success of graphene,[1,2] a family of novel two-dimensional (2D) materials have been synthesized in experiment, such as hexagonal boron nitride (h-BN),[3,4] black phosphorus (phosphorene),[5] a series of transition-metal dichalcogenides.[6−10] In particular, researchers have paid special attention to the 2D materials made by the heavy group-IV elements, such as silicene,[11−14] germanene,[15−18] and stanene, due to their novel electronic properties. Among them, silicene has been obtained successfully by molecular beam epitaxy growth, and germanene was realized by the mechanical exfoliation and molecular beam epitaxy. Since the element Sn is very heavy, stanene and its derivatives are initially considered to be impossibly synthesized in experiments.

Only very recently, a great experimental progress has been made for the synthesis of stanene. Qian *et al.* have reported the success in fabrication of 2D stanene on the substrate of Bi_2Te_3 by molecular beam epitaxy.[19] Due to the breaking of the inversion symmetry on the substrate, the hole pockets of stanene are observed at the Γ point. Similar to silicene and germanene, stanene has a buckled honeycomb lattice with a Dirac-like electronic property. In addition, stanene has its unique properties, such as the large-gap quantum spin Hall (QSH) effect, enhanced thermoelectricity and topological superconductivity. In theory, Xu *et al.* demonstrated that the 2D tin films are QSH insulators with a gap of 0.3 eV, which can be effectively tuned by the chemical functionalization.[20] Then, Ma *et al.* demonstrated that there are Dirac cone-like characteristics in the halogenated 2D tin forms at the Fermi level.[21] Inspired by these interesting findings, we are encouraged to demonstrate the geometric and electronic properties of the fully fluorinated stanene (SnF) monolayer.

There are two main reasons for choosing the SnF monolayer as our research object. Firstly, stanene in experiment has a strong interaction with the substrates of Bi_2Te_3, resulting in a metallicity problem into stanene.[19,22] Since the lack of a band gap will restrict the applications in macroelectronics, a suitable band gap is highly desired for stanene. In fact, fluorination has been proved as an effective method to generate a band gap in 2D materials, such as fluorinated graphene,[23−28] fluorinated silicene[29] and fluorinated BN.[30] Secondly, the thermodynamic stability of stanene is weak, which could only be stable at very low temperature down to 77 K in experiment. Compared with stanene, fluorination is proposed to help stabilize stanene and may offer more desirable features. Nevertheless, little is known about the electronic, mechanical and optical properties of the SnF monolayer. In this work, by means of density functional theory computations, we show theoretical evidence for the SnF monolayer, which has a considerable indirect band gap of 278 meV, due to the strong spin-orbit coupling (SOC) effect.

We have adopted the van der Waals correlated Perdew–Burke–Ernzerhof functional[31−33] for all our calculations by using the plane-wave basis set, as implemented in the Vienna ab initio simulation package (VASP).[34] The electron exchange energy is treated by the Grimme dispersion correlated exchange en-

*Supported by the Science Foundation of Nanjing University of Posts and Telecommunications under Grant No NY215064, the China Postdoctoral Science Foundation under Grant No 2015M581824, and the Jiangsu Post-doctoral Foundation under Grant No 1501070B.

**Corresponding author. Email: njustlifeng@163.com

© 2016 Chinese Physical Society and IOP Publishing Ltd

ergy (PBE-D2), and the electron–ion interactions are descried by projector augmented-wave method.[35] Kinetic-energy cutoff of 500 eV with $6 \times 6 \times 1$ k-mesh grids is good enough for convergence. A large vacuum layer of 25 Å was applied. All the structures were fully relaxed until the energy changes less than 10^{-6} eV and the forces are no more than 0.01 eV/Å. This method has been proved effective for many systems, such as graphane,[36] black phosphorus.[37] Phonon spectra were computed depending on the finite displacement method as implemented in CASTEP code.[38]

To obtain insight into the SnF monolayer, we first studied the structural properties of stanene for validation (Fig. 1(a)). The lattice constant of free standing stanene is 4.61 Å, in good agreement with another reported theoretical result of 4.67 Å, while slightly larger than that of the experimental value of 4.38 Å.[19] This difference is attributed to the compressive strain of stanene on the $Bi_2Te_3(111)$ substrate in experiment. At the DFT-D2 level, the band structure of stanene is presented in Fig. 1(b). Similar to graphene, silicene and germanene, the free-standing stanene has a Dirac cone at the fermi level, in which the valence band and conduction band are meeting at one point at the fermi level. This result could be contributed to the half-filled p_z orbitals of Sn atoms. Since the element Sn is heavy, the SOC effect cannot be ignored. When considering the SOC effect, a gap of 89 meV is opened in stanene, in good agreement with other works (100 meV).[20] This is the largest gap found in the family of the 2D group-IV nanosheets. Thus the chosen theoretical methods are reliable for stanene.

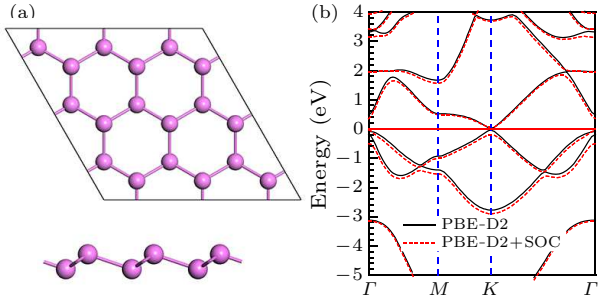

Fig. 1. (a) Top and side views of stanene in a $3 \times 3 \times 1$ supercell. (b) Band structure of stanene computed at the DFT-D2 level.

Then, we explore the ground state structure of the SnF monolayer, including configurations with chair, boat, and stirrup. Similar to the fluorinated graphene, silicene and germanene, the SnF monolayer with chair form has the most stable structure, in which F atoms are attached on both sides of the Sn skeleton. The optimized lattice constant of SnF monolayer is 4.95 Å, which is significantly larger than that of stanene (4.61 Å) by 7.4%. This could be explained by the strong electrostatic repulsion between the F atoms on the surface. Since the lattice constant is stretched, the thickness of the Sn skeleton is compressed from 0.89 Å to 0.51 Å for stanene and the SnF monolayer, respectively. The distance between the F layers is 4.44 Å. Moreover, the stability of the SnF monolayer can be confirmed by its phonon dispersion curves (Fig. 2(c)), where no appreciable imaginary phonon mode can be identified. Therefore, the SnF monolayer is kinetically stable.

To reveal the impressive effect of fluorination, the band structure of the SnF monolayer is performed within and without the SOC effect. When the SOC effect is not considered, the SnF monolayer is gapless with the valence band maximum (VBM) and the conduction band minimum (CBM) meeting at the Fermi level. When the SOC effect is involved, the valence and conduction bands degenerate at the Γ point, and a significant spin-orbit coupling has been observed in the valence band, resulting in a considerable band gap of 278 meV. In contrast with pure stanene, the direct gap at the Γ point is significantly enlarged from 89 to 381 meV for the SnF monolayer. Surprisingly, the fluorination has greatly enhanced the SOC effect in the SnF monolayer, which is not generally applicable. For example, the fluorinated graphene has a large band gap at the Γ point (>3 eV), which is negligibly affected by the SOC effect.[26] Thus the SnF monolayer is a significant QSH insulator with a large nontrivial gap of 381 meV, due to the strong SOC effect.

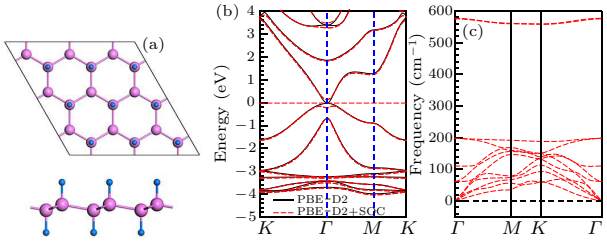

Fig. 2. (a) Top and side views of the SnF monolayer in a $3 \times 3 \times 1$ supercell. Sn and F atoms are denoted by large purple and small blue balls, respectively. (b) Band structure within and without the SOC effect are computed at the DFT-D2 level. (c) Phonon dispersion of the SnF monolayer.

To understand the origin of the SOC effect, we first computed the partial charge densities plots of the VBM and CBM for the SnF monolayer. As shown in Figs. 3(a)–3(d), the states near the fermi level are mainly contributed by the s and p_{xy} orbitals of the Sn atoms. In Fig. 3(e), the schematic diagram of the evolution of energy levels for the SnF monolayer at the Γ point is plotted, in which $s+$, $s-$ represent for s bonding and antibonding orbitals, and $p_{xy}+$, $p_{xy}-$ for p_{xy} bonding and antibonding orbitals, respectively. When the SOC is turned off (in blue box), the fermi level locates at the bonding state of $p_{xy}+$ orbital, resulting in the semimetallic property for the SnF monolayer. When the SOC is turned on (in red box), the $p_{xy}+$ state is split into $|p, \pm 3/2\rangle$ and $|p, \pm 1/2\rangle$ two states, corresponding to the total angular momentum

of $j = 3/2$ and $1/2$, respectively. Thereby, the $p_{xy}+$ state is half occupied due to it being quadruply degenerate, forming a nontrivial energy gap of 381 meV. Moreover, the partial charge densities of VBM are not only coming from the Sn atoms but also partially from the F atoms (Figs. 3(a) and 3(b)), thus both Sn and F atoms are responsible for the strong SOC effect in the SnF monolayer. In comparison, the VBM of the fluorinated graphene is totally contributed by the carbon atoms, thereby no SOC effect is obtained.

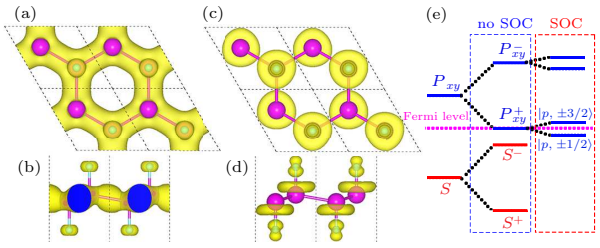

Fig. 3. Top and side views of the partial charge densities of VBM (a), (b) and CBM (c), (d), respectively. The isovalue is 0.005 e/A^3. (e) Schematic diagram of the evolution of energy levels at the Γ point for the SnF monolayer.

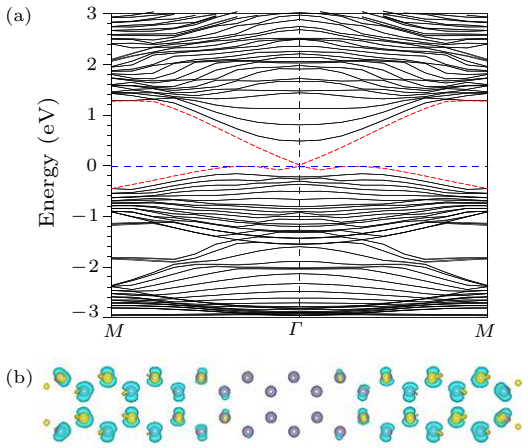

Fig. 4. (a) Band structure of armchair SnF nanoribbons with a ribbon width of 51 Å. Helical edge states are shown in red lines. (b) The charge distribution of edge states at the Γ point are visualized at the two edges of the SnF nanoribbon.

To check the existence of the edge states in the SnF monolayer, a slab modeling of an armchair SnF nanoribbon with all the edge atoms passivated by H atoms is established. A large ribbon width of 51 Å is chosen to avoid the interaction between the two edges, as well as a large enough vacuum layer of 20 Å. The band structure is shown in Fig. 4(a). It can be clearly seen that a remarkable topological edge state (as marked by the red line) is formed at the fermi level, crossing linearly at the Γ point. Moreover, we find that the charge distributions of edge states at the Γ point are located at the two edges of the SnF nanoribbon. Thus the existence of edge states indicates that the SnF monolayer is indeed a 2D topological insulator.

In addition to the electronic properties, the elastic modulus is an important physical property for a new material. To illustrate the elastic modulus, a tetragonal lattice containing four Sn and four F atoms is constructed. As shown in Fig. 5, a uniaxial elastic strain from -5% to 5% is applied for the SnF monolayer along x and y directions, respectively. It is found that the structural energy versus the strain is fitting well with the curve of the quadratic linear relation. The elastic modulus is derived from the equation of $C = [\partial^2 E/\partial\varepsilon^2]/S$, where E is the total energy of the structure, ε is the uniaxial strain, and S is the area of the unit cell. Our calculations show that the elastic moduli of the SnF monolayer along x and y directions are 19.45 J/m^2 and 19.15 J/m^2, respectively. These values are comparable to the in-plane stiffness of black phosphorus monolayer along the x direction ($\sim$28.94 J/m^2).[39] Thus, the SnF monolayer is so soft that it is suggested to be placed on suitable substrates in experiment, for example, stanene on the $Bi_2Te_3(111)$ substrate.[19]

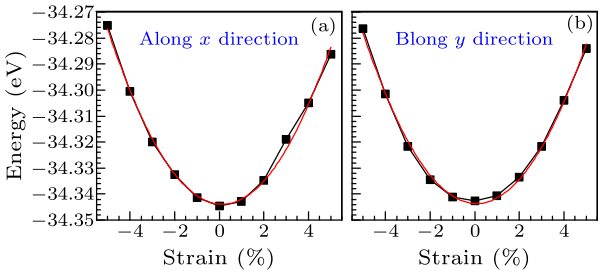

Fig. 5. Structural energy of the SnF monolayer versus the applied strain from -5% to 5% along x and y directions.

Optical properties are another important characteristic for a new material. To address the optical property, we calculate the imaginary parts of the dielectric function for stanene, the SnF monolayer and the stanene/SnF bilayer with/without the SOC effect, as presented in Fig. 6. When the SOC effect is not considered, the first peak in the visible-light region for stanene is at 419 nm. Then, the light absorption is gradually increased along with the light wavelength. When taking the SOC effect into account, the first peak in the visible-light region moves to 482 nm, followed by a sudden jump in the light absorption. This result could be explained by the band gap opening induced by the SOC effect, which plays a leading role in the optical properties. Similarly, we find that the light absorption for the SnF monolayer with the SOC effect is only half the one without the SOC effect. Since about 50% of the solar energy comes from the visible-light region, the light absorption of the SnF monolayer is weak. To enhance the visible-light activity, the stanene/SnF bilayer is constructed. Surprisingly, the stanene/SnF bilayer exhibits a remarkable visible-light absorption, with a high optical absorption peak locating at 709 nm (corresponding to 1.75 eV).

Furthermore, the light absorption of the stanene/SnF bilayer is much higher than that of the individual stanene and the SnF monolayer. This could be understood by the interlayer couplings between stanene and the SnF monolayer, which have modified the orbital projections of the bands. Therefore, the stanene/SnF bilayer has great potential applications in optoelectronics, such as sunlight absorber and sensors.

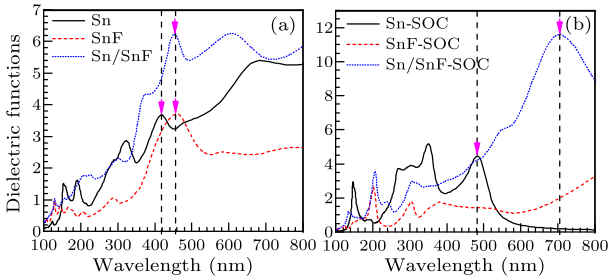

Fig. 6. Calculated imaginary dielectric functions versus the wavelength for stanene (Sn), the SnF monolayer (SnF) and the stanene/SnF bilayer (Sn/SnF).

In summary, we have theoretically investigated that fluorination has significantly modified the geometric and electronic properties of stanene. Remarkably, a significant spin-orbit coupling has been observed in the valence band at the Γ point of the SnF monolayer, with a considerable nontrivial gap of 381 meV. In addition, the SnF monolayer is soft, thus it is suggested to be placed on suitable substrates in experiment. Furthermore, the light absorption of the stanene/SnF bilayer in the visible-light region is very high, which is supposed to be an attractive sunlight absorber. These findings render the SnF monolayer a promising candidate in electronics and optoelectronics. Considering the recent progress in the experimental technology, we believe that the SnF monolayer could be realized experimentally in the near future.

The computational resources utilized in this work were provided by Shanghai Supercomputer Center.

References

[1] Novoselov K S, Geim A K, Morozov S V, Jiang D, Zhang Y, Dubonos S V, Grigorieva I V and Firsov A A 2004 *Science* **306** 666
[2] Novoselov K S, Geim A K, Morozov S V, Jiang D, Katsnelson M I, Grigorieva I V, Dubonos S V and Firsov A A 2005 *Nature* **438** 197
[3] Zeng H B, Zhi C Y, Zhang Z H, Wei X L, Wang X B, Guo W L, Bando Y and Golberg D 2010 *Nano Lett.* **10** 5049
[4] Levendorf M P, Kim C J, Brown L, Huang P Y, Havener R W, Muller D A and Park J 2012 *Nature* **488** 627
[5] Abbas A N, Liu B, Chen L, Ma Y, Cong S, Aroonyadet N, Köpf M, Nilges T and Zhou C 2015 *ACS Nano* **9** 5618
[6] Wang Q H, Kalantar-Zadeh K, Kis A, Coleman J N and Strano M S 2012 *Nat. Nanotechnol.* **7** 699
[7] Yin Z, Li H, Li H, Jiang L, Shi Y, Sun Y, Lu G, Zhang Q, Chen X and Zhang H 2012 *ACS Nano* **6** 74
[8] Miwa J A, Dendzik M, Grønborg S S, Bianchi M, Lauritsen J V, Hofmann P and Ulstrup S 2015 *ACS Nano* **9** 6502
[9] Radisavljevic B, Radenovic A, Brivio J, Giacometti V and Kis A 2011 *Nat. Nanotechnol.* **6** 147
[10] Yoon Y, Ganapathi K and Salahuddin S 2011 *Nano Lett.* **11** 3768
[11] Lalmi B, Oughaddou H, Enriquez H, Kara A and Vizzini S 2010 *Appl. Phys. Lett.* **97** 223109
[12] Houssa M, Pourtois G, Afanas'ev V V and Stesmans A 2010 *Appl. Phys. Lett.* **97** 112106
[13] Vogt P, De Padova P, Quaresima C, Avila J, Frantzeskakis E, Asensio M C, Resta A, Ealet B and Le Lay G 2012 *Phys. Rev. Lett.* **108** 155501
[14] Feng B J, Ding Z J, Meng S, Yao Y G, He X Y, Cheng P, Chen L and Wu K H 2012 *Nano Lett.* **12** 3507
[15] Kaloni T P and Schwingenschlögl U 2013 *Chem. Phys. Lett.* **583** 137
[16] Li L Y and Zhao M W 2013 *Phys. Chem. Chem. Phys.* **15** 16853
[17] Bianco E, Butler S, Jiang S S, Restrepo O D, Windl W and Goldberger J E 2013 *ACS Nano* **7** 4414
[18] Li L F, Lu S Z, Pan J B, Qin Z H, Wang Y Q, Wang Y L, Cao G Y, Du S X and Gao H J 2014 *Adv. Mater.* **26** 4820
[19] Zhu F F, Chen W J, Xu Y, Gao C L, Guan D D, Liu C H, Qian D, Zhang S C and Jia J F 2015 *Nat. Mater.* **14** 1020
[20] Xu Y, Yan B H, Zhang H J, Wang J, Xu G, Tang P Z, Duan W H and Zhang S C 2013 *Phys. Rev. Lett.* **111** 136804
[21] Ma Y D, Dai Y, Guo M, Niu C W and Huang B B 2012 *J. Phys. Chem.* C **116** 12977
[22] Ding Y and Wang Y L 2015 *J. Phys. Chem.* C **119** 27848
[23] Robinson J T, Burgess J S, Junkermeier C E, Badescu S C, Reinecke T L, Perkins F K, Zalalutdniov M K, Baldwin J W, Culbertson J C, Sheehan P E and Snow E S 2010 *Nano Lett.* **10** 3001
[24] Samarakoon D K, Chen Z F, Nicolas C and Wang X Q 2011 *Small* **7** 965
[25] Jeon K J, Lee Z, Pollak E, Moreschini L, Bostwick A, Park C M, Mendelsberg R, Radmilovic V, Kostecki R, Richardson T J and Rotenberg E 2011 *ACS Nano* **5** 1042
[26] Şahin H, Topsakal M and Ciraci S 2011 *Phys. Rev.* B **83** 115432
[27] Kashtiban R J, Dyson M A, Nair R R, Zan R, Wong S L, Ramasse Q, Geim A K, Bangert U and Sloan J 2014 *Nat. Commun.* **5** 4902
[28] Zhou J, Wu M M, Zhou X and Sun Q 2009 *Appl. Phys. Lett.* **95** 103108
[29] Ding Y and Wang Y 2012 *Appl. Phys. Lett.* **100** 083102
[30] Zhou J, Wang Q, Sun Q and Jena P 2010 *Phys. Rev.* B **81** 085442
[31] Heyd J, Scuseria G E and Ernzerhof M 2006 *J. Chem. Phys.* **124** 219906
[32] Heyd J, Scuseria G E and Ernzerhof M 2003 *J. Chem. Phys.* **118** 8207
[33] Paier J, Marsman M, Hummer K, Kresse G and Gerber I C 2006 *J. Chem. Phys.* **124** 154709
[34] Kresse G and Furthmuller J 1996 *Phys. Rev.* B **54** 11169
[35] Perdew J P, Burke K and Ernzerhof M 1996 *Phys. Rev. Lett.* **77** 3865
[36] Jiang S S, Arguilla M Q, Cultrara N D and Goldberger J E 2015 *Acc. Chem. Res.* **48** 144
[37] Qiao J S, Kong X H, Hu Z X, Yang F and Ji W 2014 *Nat. Commun.* **5** 4475
[38] Segall M D, Philip J D L, Probert M J, Pickard C J, Hasnip P J, Clark S J and Payne M C 2002 *J. Phys.: Condens. Matter* **14** 2717
[39] Xiao J, Long M Q, Zhang X J, Ouyang J, Xu H and Gao Y L 2015 *Sci. Rep.* **5** 09961